

We are IntechOpen, the world's leading publisher of Open Access books Built by scientists, for scientists

6,900

Open access books available

186,000

International authors and editors

200M

Downloads

Our authors are among the

154

Countries delivered to

TOP 1%

most cited scientists

12.2%

Contributors from top 500 universities



WEB OF SCIENCE™

Selection of our books indexed in the Book Citation Index
in Web of Science™ Core Collection (BKCI)

Interested in publishing with us?
Contact book.department@intechopen.com

Numbers displayed above are based on latest data collected.
For more information visit www.intechopen.com



Dynamic Joint Passivization for Bipedal Locomotion

Shohei Kato and Minoru Ishida
Nagoya Institute of Technology
Japan

1. Introduction

A lot of research on humanoid robots or biped robots has been conducted. This research focused on enabling robots to walk very smoothly, similar to the way humans walk, which is highly energy efficient. Motion control using a central pattern generator (CPG) has attracted much attention as an effective control mechanism for biped robots to achieve human-like walking (e.g., Kato & Itoh (2005); Kotosaka & Schaal (2000); Miyakoshi et al. (1998); Taga (1995a;b); Taga et al. (1991)). The CPG is modeled mathematically to a neural rhythm generator that exists at a relatively low level of the central nervous system, such as the spinal cord of animals. This motion control using the CPG has generated various motions: walking by Ishida et al. (2009a;b); Itoh et al. (2004); Nakamura et al. (2005); Taki et al. (2004), step by Miyakoshi et al. (1998), and drum motions by Kotosaka & Schaal (2000). Taga (1995a;b) proposed a neuro-musculo-skeletal model based on the CPG, and it enabled a biped robot to have a human gait in two dimensions. Among the researchers of highly energy-efficient walking, McGeer (1990) was the first to study passive dynamic walking (PDW). A PDW robot walks forward by placing the foot on the ground and riding on the supporting leg, which rolls forward as an inverted pendulum mounted on the supporting foot. At the same time, it places the swing foot forward by moving the swing leg in a pendular arc, so that it makes the foot strike a ground when the mechanism is in a configuration identical to that at the beginning of a step. If the dynamic characteristic of the robot and the environment (e.g., the slope and velocity when the walking begins) agree, then the PDW robot achieves highly energy-efficient walking without any actuator control. Sugimoto & Osuka (2004) proposed a control method for quasi passive dynamic walking (Quasi-PDW). Quasi-PDW means that the robot usually does PDW without any input torque, and the actuators of the robot are used for ensuring walking stability only when the walking begins or when a disturbance occurs. Haruna et al. (2001) researched a PDW robot with a torso. CPG-based motion control inputs some torque to all the joints of the robot's lower limbs regardless of gait. When we think about human walking, we take into account the joints of the swing leg without any input torque. Active walking needs to be mixed with PDW for robot walking. Quasi-PDW is an example of a mixture of active walking and PDW. Quasi-PDW is applicable to the robot whose dynamic characteristic suits to PDW. However, there is a lot of robots that can not satisfy a dynamic characteristic for PDW. To achieve this mixture with the robots, we added the mechanism of PDW to an active walking robot. In this chapter, we describe a motion control method based on the mixture of CPG and PDW (Ishida et al. (2009a;b)), that is, the

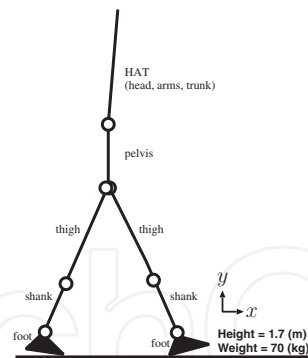


Fig. 1. Link Structure of Robot (2D).

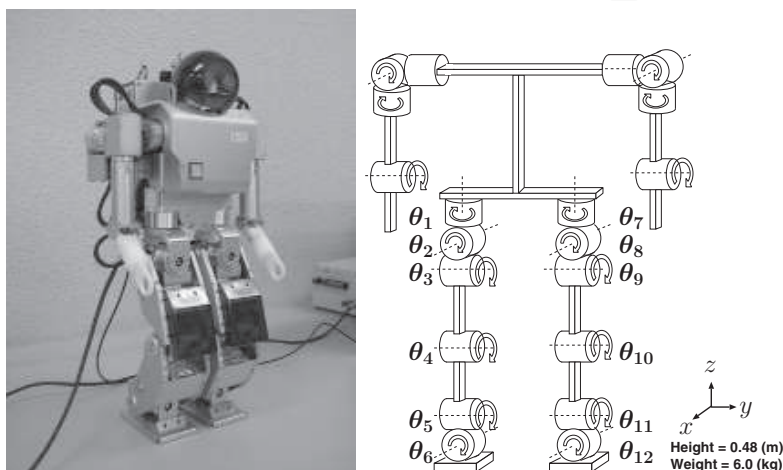


Fig. 2. HOAP-1 (left) and Its Link Structure (right).

dynamic passivization of joint control, achieving robust and energy-efficient walking. We focused on robot walking on a downhill slope.

2. The Robot model and its motion control primitive

2.1 The link structure of humanoid robot

The section describes two link models of humanoid robot: two dimensional link model in sagittal plane and three dimensional link model of entire body.

2.1.1 Two dimensional model

The model of the human body is composed of the HAT (head, arms, and trunk), pelvis, thighs, shanks, and feet (shown in Figure 1). There are seven joints, two each at the hips, knees, and ankles, and one at the trunk.

2.1.2 Three dimensional model

We also consider the motion control of a humanoid robot, HOAP-1 (Murase et al. (2001)), shown in Figure 2. HOAP-1 has 6-DOFs in each leg. The coxa joint has three degrees of freedom; pitch, yaw, and roll, the knee joint has one degree of freedom; pitch, and the ankle joint has two degrees of freedom; pitch, and roll. The height and weight of the robot and 48[cm] and 6[kg].

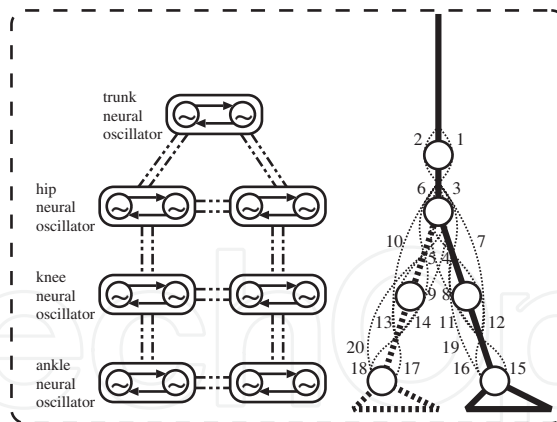


Fig. 3. The neural system (left) and the musculo-skeletal system (right) (two dimensional version).

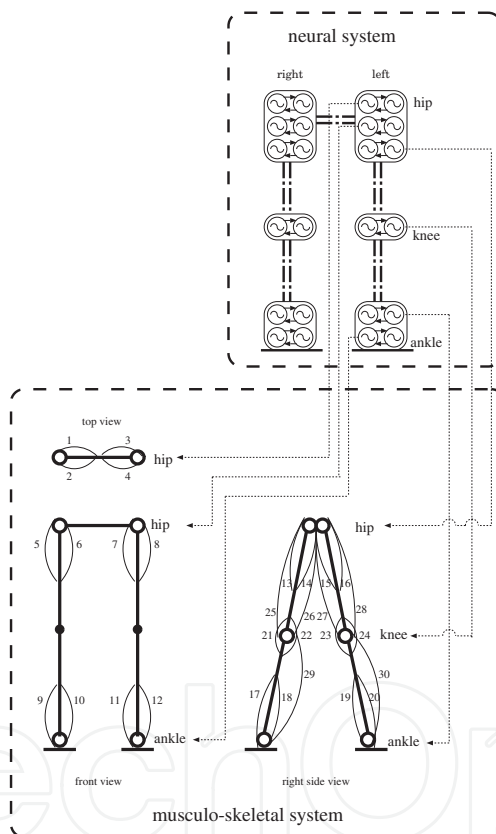


Fig. 4. The neural system and the musculo-skeletal system (three dimensional version).

2.2 Neural rhythm generator

Walking movement is periodical. In this research, we control walking movement using CPG, which is often used in generating periodical movement. CPG is modeled mathematically to the neural rhythm generator which exists at a relatively low level of the central nervous system such as the spinal cord of animals. Standout feature of CPG, it is synchronized its inner state with rhythmic input from outside in term of phase. Using this feature, therefore walking movement having robustness for changes of environment is able to be generated. CPG is composed of multi-neurons which inhibit each other. The mathematical model of a

neuron is represented as following system of differential equation.

$$\tau_i \dot{u}_i = -u_i - b \cdot f(v_i) + \sum_{j=1}^n w_{ij} f(u_j) + u_0 + S_i, \quad (1)$$

$$\tau'_i \dot{v}_i = -v_i + f(u_i), \quad (2)$$

$$f(x) = \max(x, 0), \quad (3)$$

where u_i is the inner state of i -th neuron; v_i is a variable which represents the degree of the adaptation or self-inhibition effect of the i -th neuron; τ_i and τ'_i are time constants of the inner state and the adaptation effect of the i -th neuron, respectively; b is a coefficient of the adaptation effect; w_{ij} is a connecting weight from the j -th neuron to the i -th neuron; u_0 is an external input with a constant rate; and S_i is the local and global sensory information that is sent to the i -th neuron. A neuron excited by u_0 is oscillated by self-inhibition and cross-inhibition, and $f(u)$ is output of neuron. For more precise, please refer to Matsuoka (1985) and Matsuoka (1987).

2.3 Neuro-musculo-skeletal system

In this research, we adopted the neuro-musculo-skeletal system proposed by Taga (1995a) for a motion control method based on CPG in the robot. The neuro-musculo-skeletal system is composed of two dynamical systems: a neural system and a musculo-skeletal system. The neural system is composed of CPG network, and the musculo-skeletal system is composed of skeletons considered muscles surrounding to them. The system can generate flexible and adaptable walking movement through the mutual interaction among the neural system, the musculo-skeletal system and environment.

In this chapter, we propose CPG-based walking motion generation considering two styles in neuro-musculo-skeletal system: walking in sagittal plane (in two dimensions) and walking with real lower body (in three dimensions).

2.3.1 Two dimensional model

In the neural system, the neural rhythm generator consists of seven neural oscillators in accordance with the robot's link structure shown in Figure 1. The neural oscillators are allocated to seven joints: the trunk and the pairs of the hips, knees, and ankles, shown in Figure 3 (left). Two neurons at a neural oscillator each have a flexion and extension effect on muscles corresponding to the CPG. In the musculo-skeletal system, the skeletons match the robot's link structure. There are six single-joint muscles and three double-joint muscles for each of the limbs and two for the upper body. Figure 3 (right) shows the configuration of the muscles. Two neurons in the neural oscillators alternately activate the antagonist muscles.

2.3.2 Three dimensional model

For the three dimensional link model (see Figure 2 (left)), neural oscillators are allocated to twelve joints: the pairs of the coxas (pitch, yaw, and roll), knees, and ankles (pitch and roll). Two neurons at a neural oscillator each have a flexion and extension effect on muscles corresponding to the CPG. In the musculo-skeletal system, the skeletons match the robot's link structure. There are twelve single-joint muscles and three double-joint muscles for each of the limbs. Figure 4 shows the configuration of the muscles (30 muscles in total).

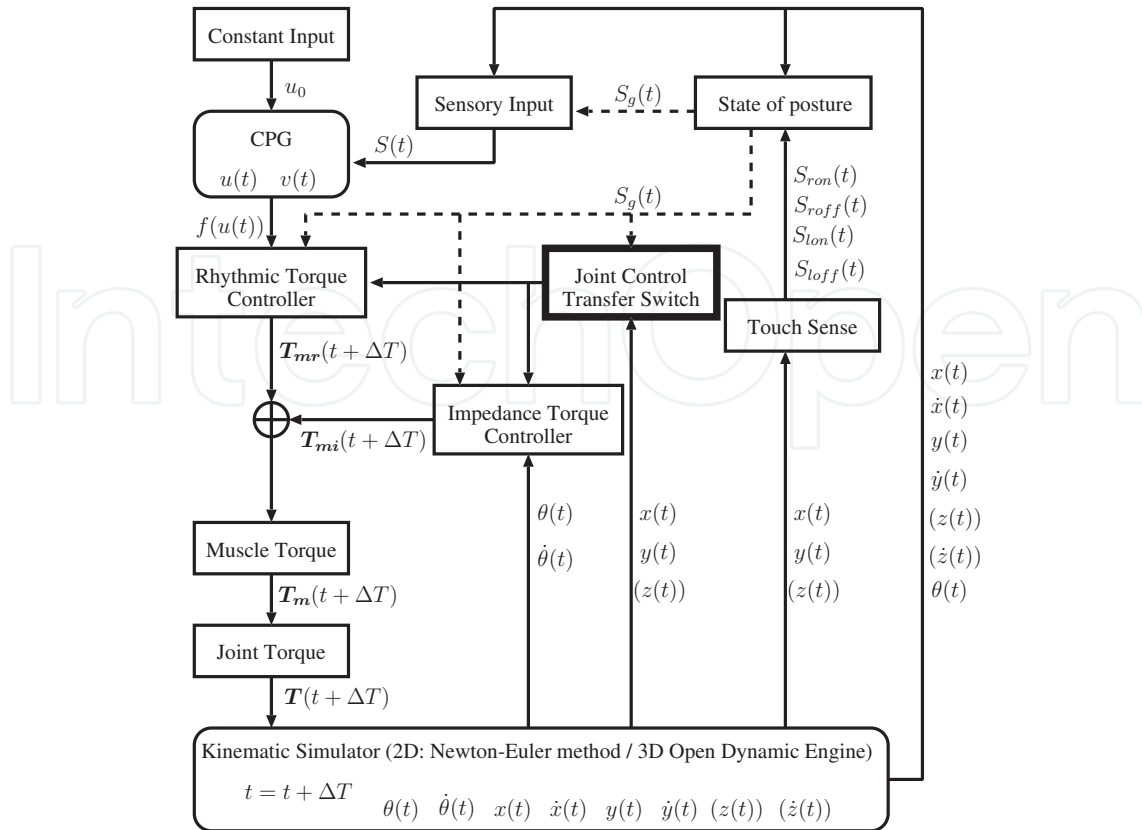


Fig. 5. Block diagram of motion control system based on dynamic passivization of joint control

2.4 Motion control based on neuro-musculo-skeletal system

Figure 5 shows a block diagram of the motion control system based on the dynamic passivization of joint control. In this research, we added a joint control transfer switch to the neuro-musculo-skeletal system proposed by Taga for a motion control method. Joint control transfer switch is described in Section 3.1. If the transfer switch is passive, then it nullifies the input torque in the swing leg for the rhythmic torque controller and for the impedance torque controller. If it is active, then it enables the input torque in the swing leg for the rhythmic torque controller and for the impedance torque controller. The system performs the motion control based on the iteration of the following processes:

1. First, output $f(u(t))$ of the CPG in time t is excited by constant input u_0 to the neuron. The rhythmic torque controller generates rhythmic torque $T_{mr}(t + \Delta T)$ from $f(u(t))$, sensory input $S(t)$ of the robot at time t , and the output of the joint control transfer switch in time t .
2. The impedance torque controller generates impedance torque $T_{mi}(t + \Delta T)$ to maintain a standing position from joint angle $\theta(t)$, joint angular velocity $\dot{\theta}(t)$, and the sensory input of the robot at time t .
3. The muscle torque $T_m(t + \Delta T)$ is generated from $T_{mr}(t + \Delta T)$ and $T_{mi}(t + \Delta T)$.
4. The joint torque $T(t + \Delta T)$ is calculated from $T_m(t + \Delta T)$.
5. The kinematics simulator generates the motion of the robot when joint torque $T(t + \Delta T)$ is given to the robot. Then, the simulator calculates joint angle $\theta(t + \Delta T)$, joint angular

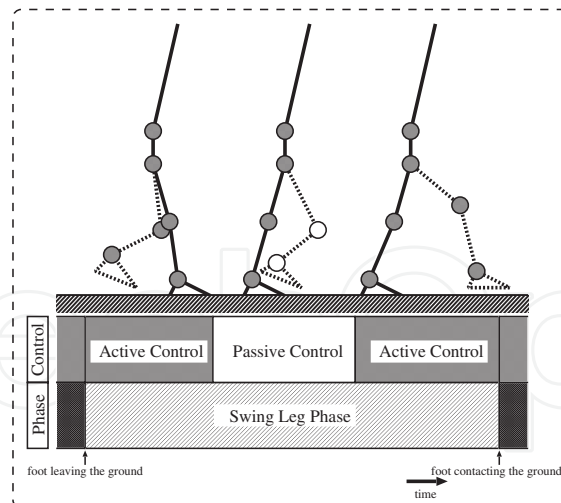


Fig. 6. Dynamic passivization of joint control

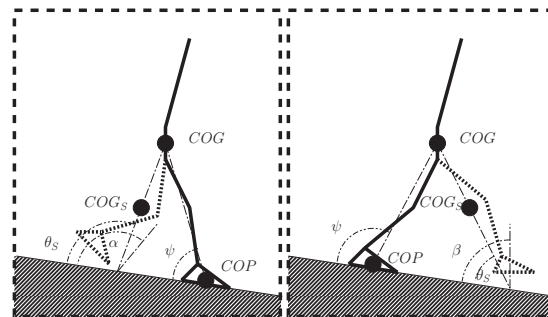


Fig. 7. Postures while walking

velocity $\dot{\theta}(t + \Delta T)$, the coordinates $p(t + \Delta T) = (x(t + \Delta T), y(t + \Delta T))^T$ ($p(t + \Delta T) = (x(t + \Delta T), y(t + \Delta T), z(t + \Delta T))^T$ for 3D simulation), and velocity $\dot{x}(t + \Delta T)$, $\dot{y}(t + \Delta T)$ ($\dot{z}(t + \Delta T)$ for 3D simulation) of each link after motion. The simulator sets the time forward for ΔT .

- The flags of the foot contacting the ground S_{ron} , S_{roff} , S_{lon} , S_{loff} are obtained by the touch sense. The state of posture $S_g(t)$ is updated by them and by the output of the kinematics simulator.

3. Dynamic passivization of joint control

In this paper, we describe a “Joint Control Transfer Switch” that is switched to “ACTIVE” or “PASSIVE” according to the environment and the posture information for adding the mechanism of PDW to the motion control method based on CPG. Our intention was to make the joint control of the swing leg temporarily passive in the swing leg phase. Figure 6 shows a concept chart of the dynamic passivization of the joint control. The important part is the passive phase time and the switch timing of the joint control.

3.1 Joint control transfer switch

The slope and posture information is used as information that decides the switch timing of the joint control (see Figure 7). The body’s center of gravity (COG) and the swing leg’s center of gravity (COG_s) are obtained from the posture information while walking. Angle θ_s is

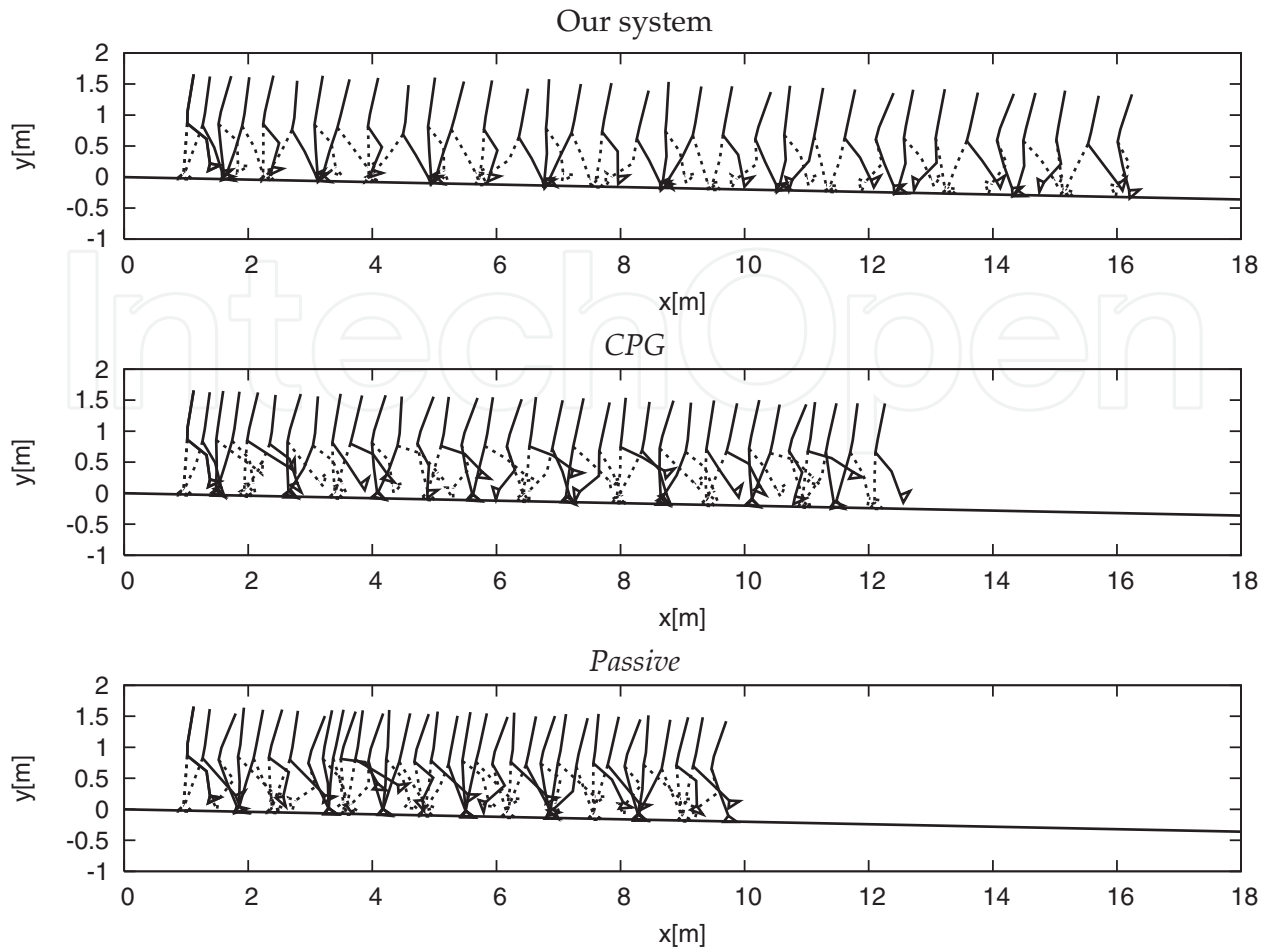


Fig. 8. Snapshots of gaits on 2 percent downhill slope with our system (top), *CPG* (middle), and *Passive* (bottom)

calculated from the *COG*, *COG_S*, and the slope. In addition, angle ψ is calculated from the *COG*, center of pressure (*COP*), and the slope.

The joint control transfer switch changes joint control to active or passive according to the following conditions:

- $\psi \leq \frac{\pi}{2}$
 - $\theta_S \geq \alpha$: ACTIVE
 - $\theta_S < \alpha$: PASSIVE
- $\psi > \frac{\pi}{2}$
 - $\theta_S > \beta$: PASSIVE
 - $\theta_S \leq \beta$: ACTIVE,

where α and β are set to an appropriate value according to a dynamic characteristic of the robot and a slope ($0 \leq \alpha, \beta \leq \pi$).

4. Walking in sagittal plane

We conducted a walking control experiment to test the effectiveness of our method. Firstly, this section reports walking control performances in sagittal plane using 2D link model shown in Figure 1. In the experiments, we used the neuro-musculo-skeletal system proposed by Taga

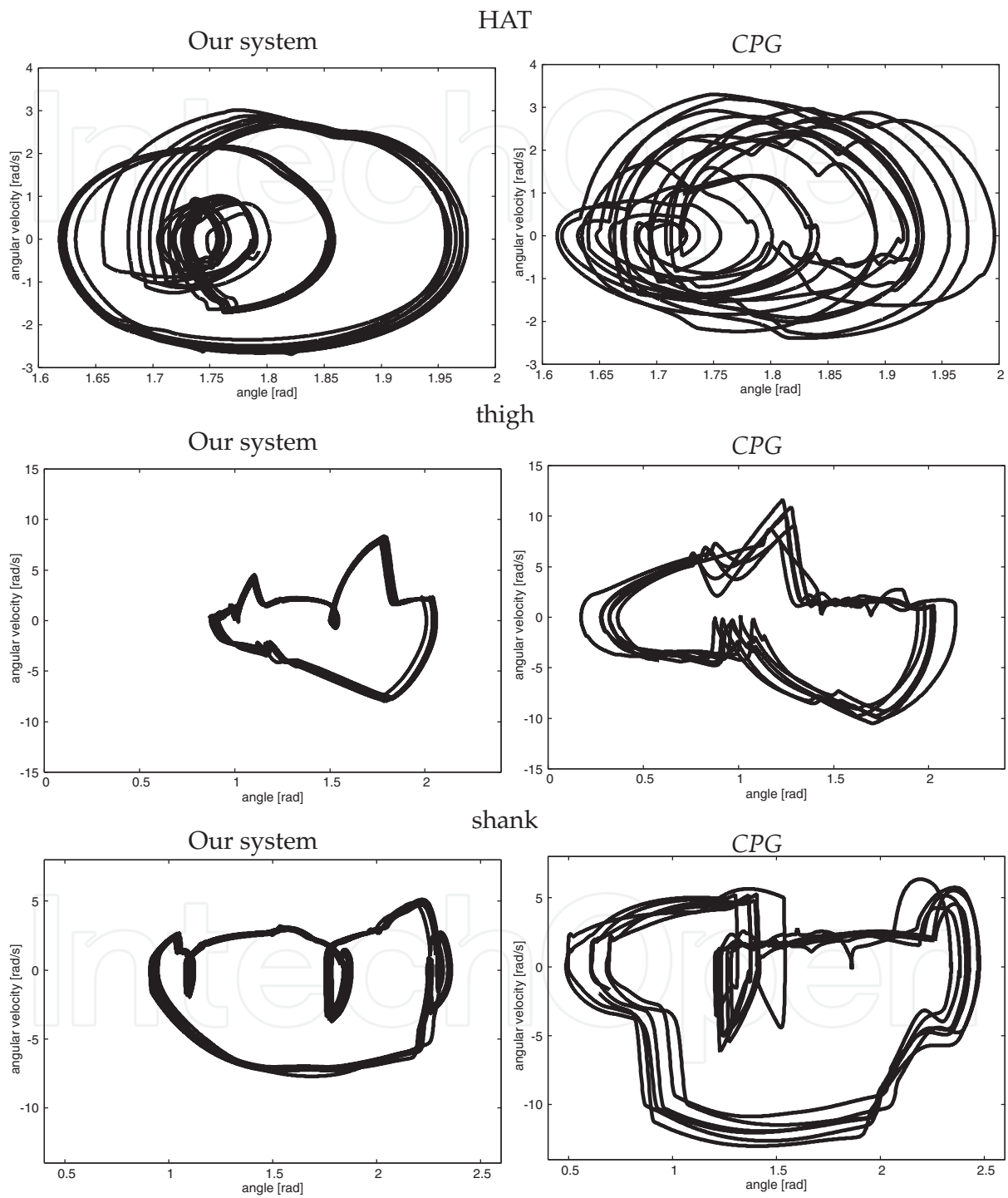


Fig. 9. Phase plots with our system (left) and *CPG* (right)

	Our system	CPG	Passive
Travel distance [m]	15.4	11.7	9.6
Sum total of input torque [Nms]	2.1E+03	2.2E+03	1.6E+03
Locomotion cost [Ns]	1.4E+02	1.9E+02	1.6E+02
α [rad]	1.79	-	-
β [rad]	0.24	-	-

Table 1. Results of first experiment

	Our system	CPG
$\lambda_{1\theta_1}$ (HAT)	7.5E-02	1.1E-01
$\lambda_{1\theta_2}$ (pelvis)	9.3E-03	1.3E-02
$\lambda_{1\theta_3}$ (right thigh)	1.0E-01	2.3E-01
$\lambda_{1\theta_4}$ (left thigh)	1.6E-01	2.3E-01
$\lambda_{1\theta_5}$ (right shank)	1.2E-01	2.7E-01
$\lambda_{1\theta_6}$ (left shank)	2.2E-01	2.4E-01
$\lambda_{1\theta_7}$ (right foot)	1.0E-01	1.5E-01
$\lambda_{1\theta_8}$ (left foot)	1.7E-01	1.4E-01
average	1.2E-01	1.7E-01

Table 2. Maximum lyapunov exponent

and a control method where the joint control was set to passive during the swing leg phase for comparison with our method. The former method is labeled "CPG" and the latter method is labeled "Passive". Because this robot could not do PDW in this environment, PDW was excluded from the objects of comparison.

4.1 Optimizing parameters

We optimized the common parameters of all the methods and parameters (α and β) of our method with simulated annealing with advanced adaptive neighborhood (SA/AAN) by Miki et al. (2002) prior to conducting the walking experiments (e.g., Itoh et al. (2004); Nakamura et al. (2005); Taki et al. (2004)). We optimized the rhythmic torque parameter as common parameters of all the methods. The rhythmic torque Tmr_j that acts on j -th muscle is defined by the following equation:

$$Tmr_j = (r_{part} \cdot S_{on} + (1 - r_{part}) \cdot S_{off}) \cdot p_{part} \cdot f(u_i), \quad (4)$$

where r and p are rhythmic torque parameter, $part$ is a type of muscle, $S_{on}(S_{off})$ is flag of the contacting (leaving) the ground. In the experiments, the walking time and the locomotion cost were used for optimizing the performance. The value of the locomotion cost is defined by the following equation:

$$Cost = \frac{1}{L} \sum_{i=1}^M \int_0^{Time} |T_i(t)| dt, \quad (5)$$

where T_i is the input torque of the i -th joint, L is the travel distance, M is the number of joints, and $Time$ is the simulation time. We perturbed parameters 10,000 times simultaneously. Each simulation took 10 seconds. We set the value of reference in Taga (1995a) for the common parameters of all the methods other than rhythm torque parameter.

4.2 Generating locomotion based on the dynamic passivization of joint control

First of all, we determined the effects of the dynamic passivization of the joint control. In this experiment, we used a 2 percent downhill slope.

Figure 8 shows the gaits over 10 seconds on a 2 percent downhill slope. In this figure, the snapshots of the gait were traced every 0.3 seconds. Table 1 shows the travel distances, the sum total of the input torques, the locomotion costs, and the parameters of our method (α and β). Our system's walks were longer than the other's. Two methods, our system and the *Passive* system, having the mechanism of passivization of joint control generated walking that was more energy efficient than that of *CPG*. When our system is compared with the *Passive* system, we found that our system consumed more torque because its passive phase time was shorter. However, the travel distance increased more than the increment of the consumption torque, and our system reduced the locomotion cost.

4.3 Gait stability analysis

Next, we determined the gait stability. In this section, the two motion control methods of our system and *CPG* were used. In the following experiments, the *Passive* system was excluded from the comparison because it is a special example of our system and our system reduced the locomotion cost more than the *Passive* system in section 4.2. Figure 9 shows the phase plots of parts of the body in the frontal plane for 9.0 seconds from 1.0 second after the walking begins: the HAT (head, arms, and trunk) (top), the thigh of right leg (middle), and the shank of right leg (bottom). The horizontal axes represent the absolute angle in the radian, and the vertical axes represent the angular velocities. Our system generates steady periodic motion because its phase plots are more periodic than those of *CPG*.

We analyzed the gait stability using the maximum lyapunov exponent. Table 2 shows the maximum lyapunov exponent (Alligood et al. (1996)) of parts of the body. In this table, the maximum lyapunov exponents of our system's gait are smaller than those of *CPG*. The walking using our system is steadier than the *CPG*.

4.4 Adaptive walking on various slopes

The performance of the systems on various downhill slopes was then examined at a 2 percent interval with a 0 to 18 percent downhill slope. In this section, the parameters were optimized beforehand in each environment.

The experimental results demonstrated that our system and the *CPG* can walk for 10 or more seconds on downhill slopes with a 0 to 16 percent downhill. Our system and the *CPG* could not walk for 10 or more seconds on a 18 percent downhill slope. Figure 10 shows the gaits over 10 seconds on a 16 percent downhill slope. In this figure, the snapshots of the gait were traced every 0.3 seconds. Our system walks farther than *CPG* on a 16 percent downhill slope, as the results in the preceding section also indicate. Figure 11 shows the locomotion cost of each method on each downhill slope. Our system generates the energy-efficient walking on each downhill slope if it can walk for 10 or more seconds. Figure 12 shows the parameters (α , β , the maximum value of θ_S (θ_S^{max}), and the minimum value of θ_S (θ_S^{min})) on each downhill slope. If α exceeds θ_S^{max} (14 and 16 percent downhill slopes), the joint control transfer switch changes the joint control to passive at the same time the foot leaves the ground. If β falls below θ_S^{min} (2, 10, 14, 16 percent downhill slope), the joint control transfer switch changes the joint control to active at the same time as the foot touches the ground. Our system generates energy-efficient walking on various (from 0 to 12 percent) downhill slopes because it uses the

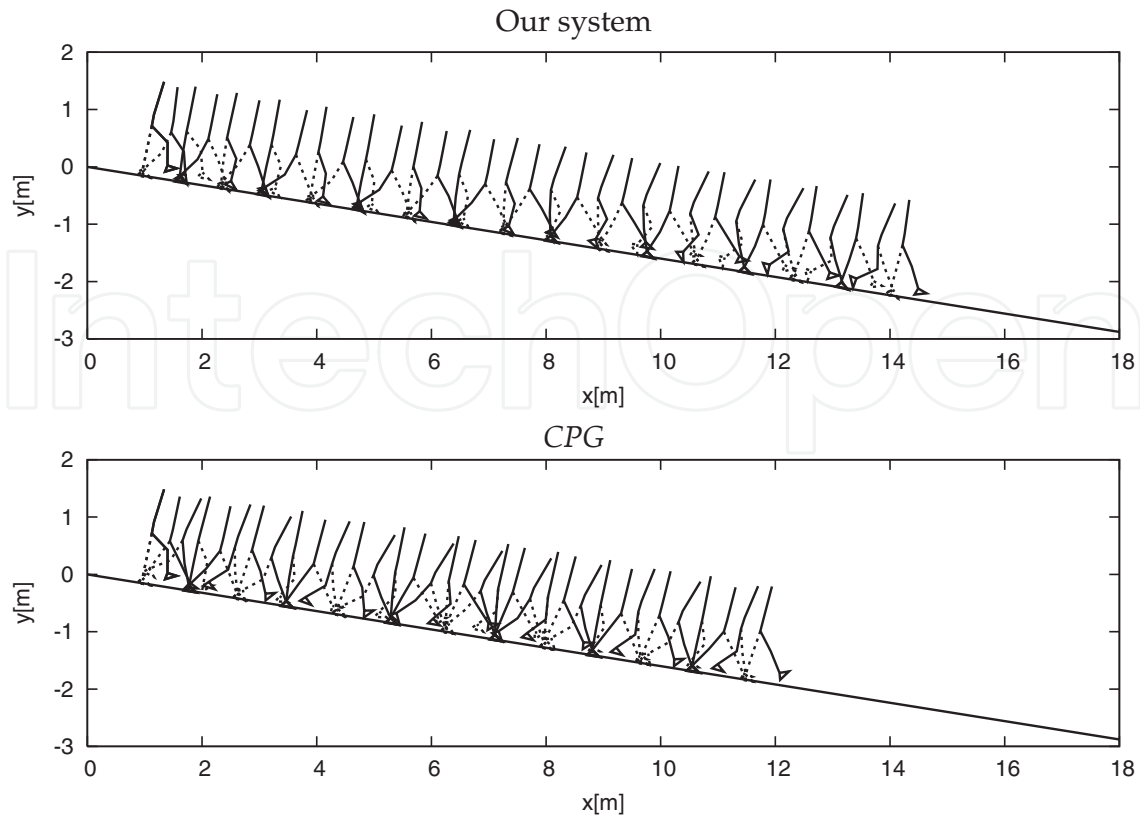


Fig. 10. Snapshots of gaits on 16 percent downhill slope with our system (top) and CPG (bottom)

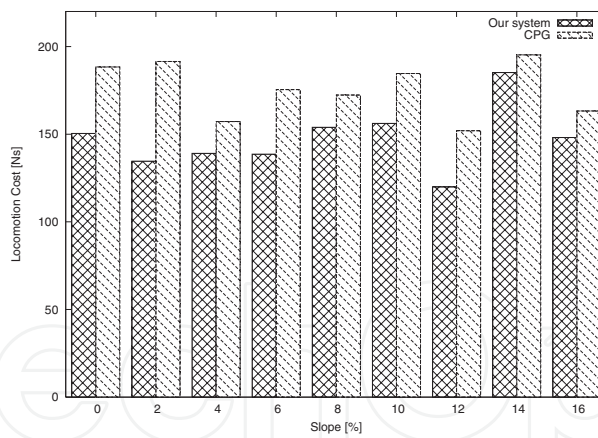


Fig. 11. Locomotion costs

passive phase appropriately. Our system generates walking that has been made passive on a 14 or 16 percent downhill slope for all periods of the swing leg phase.

4.5 Adaptive walking on uneven terrain

Next, we conducted a walking control experiment on uneven terrain. The profile of the downhill slope $y_g(x)$ is described by

$$y_g(x) = \begin{cases} -0.02x & (x < x_0) \\ -a(x - x_0) - 0.02x_0 & (x \geq x_0), \end{cases} \quad (6)$$

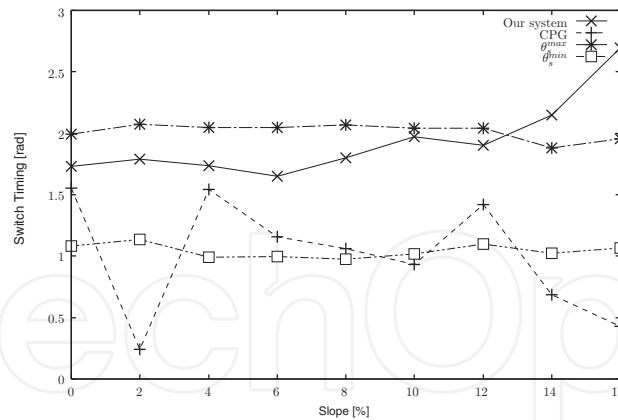


Fig. 12. Parameters of our method

a	variation	Our system	CPG
0	-0.0200	✓	✓
0.0025	-0.0175	✓	✓
0.0050	-0.0150	✓	✓
0.0075	-0.0125	✓	✓
0.0100	-0.0100	✓	×
0.0125	-0.0075	✓	✓
0.0150	-0.0050	✓	✓
0.0175	-0.0025	✓	×
0.0200	0	✓	×
0.0225	0.0025	✓	×
0.0250	0.0050	✓	×
0.0275	0.0075	✓	✓
0.0300	0.0100	✓	✓
0.0325	0.0125	✓	×
0.0350	0.0150	×	×
0.0375	0.0175	×	×
0.0400	0.0200	×	×

Table 3. Results of walking experiment on uneven terrain

where a ($0 \leq a \leq 4$) is the slope of the terrain at a 0.0025 interval, and x_0 is the position at which the slope of the terrain changes. In this experiment, we set $x_0 = 5$. We used each parameter that was obtained in the preceding section. Table 3 shows the experimental results. In this table, “✓” indicates that the robot could walk for 10 or more seconds. “×” means that the robot could not walk for 10 or more seconds; it fell down. Our system has robustness that is as good as CPG’s on uneven terrain. We found that our system did not detract from the robustness of CPG. Figure 13 shows the gaits over 10 seconds; $a = 0.0325$. In this figure, the snapshots of the gaits are traced every 0.3 seconds. Our system performs gaits that are more stable than those of CPG.

4.6 Comparing robot gait with human gait

Finally, we compared the robot and human gaits. The data on the human gait were measured using motion capture.

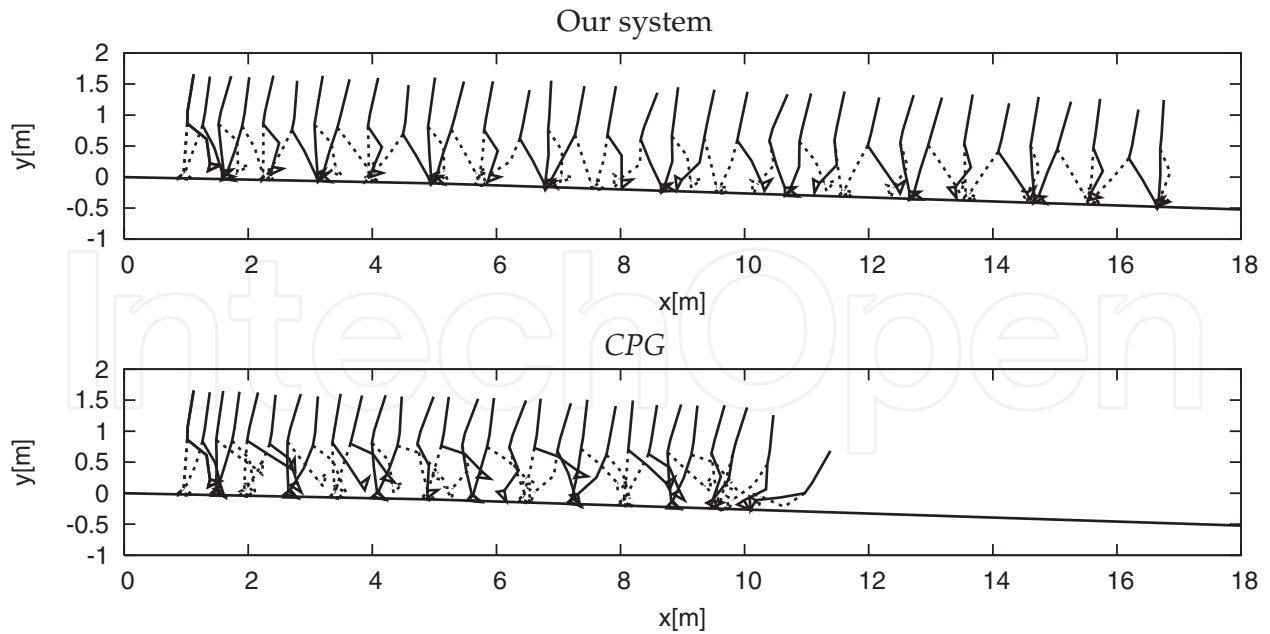


Fig. 13. Snapshots of gaits on uneven terrain with our proposed (top) and *CPG* (bottom)

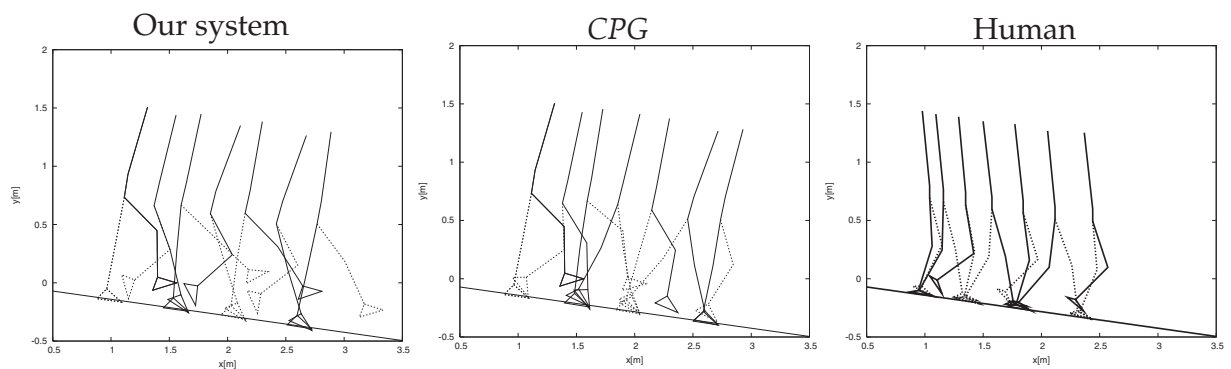


Fig. 14. Snapshots of gaits on 14 percent downhill slope with our system (left), *CPG* (center), and Human (right)

Figure 14 shows the gait over 2 seconds on a 14 percent downhill slope. In this figure, the snapshots of the gait were traced every 0.3 seconds. The our system's and *CPG*'s gaits are vorlage. In contrast, human's gait is backward tilting.

The error of the vertical component of the COG's trajectory for the robot gait and that for the human gait were calculated. Figure 15 shows the trajectories of the COG. In this figure, the trajectory of our system's gait is closer to the trajectory of a human gait than the *CPG*'s, and it is more periodically steady than *CPG*'s as well. The mean absolute error of our system is 0.0122[m], and that of *CPG* is 0.0285[m]. Our system's gait is closer to a human gait than *CPG*'s.

5. Three dimensional bipedal walking

In this section, for the expansion of the sophisticated *CPG*-*PDW*-mixture based motion control mechanism, we describe a motion control method for three dimensional biped robots shown in Figure 2 using dynamic passivization of the joint control. The motion control primitive and

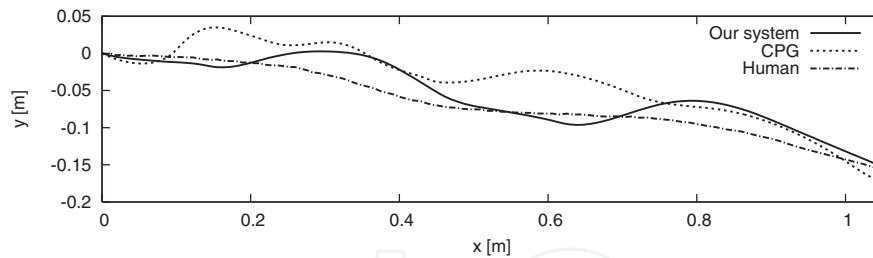


Fig. 15. Trajectories of COG

	Our system	CPG
Travel distance[m]	0.507	0.411
Sum total of input torque[Nms]	102.2	93.34
Locomotion cost[Ns]	201.8	227.2

Table 4. Results of First Experiment (3D walk)

the dynamic passivization mechanism and their parameters optimization are in an analogous manner of two dimensional way (described in Section 2 and Section 3).

5.1 Generating locomotion based on the dynamic passivization of joint control

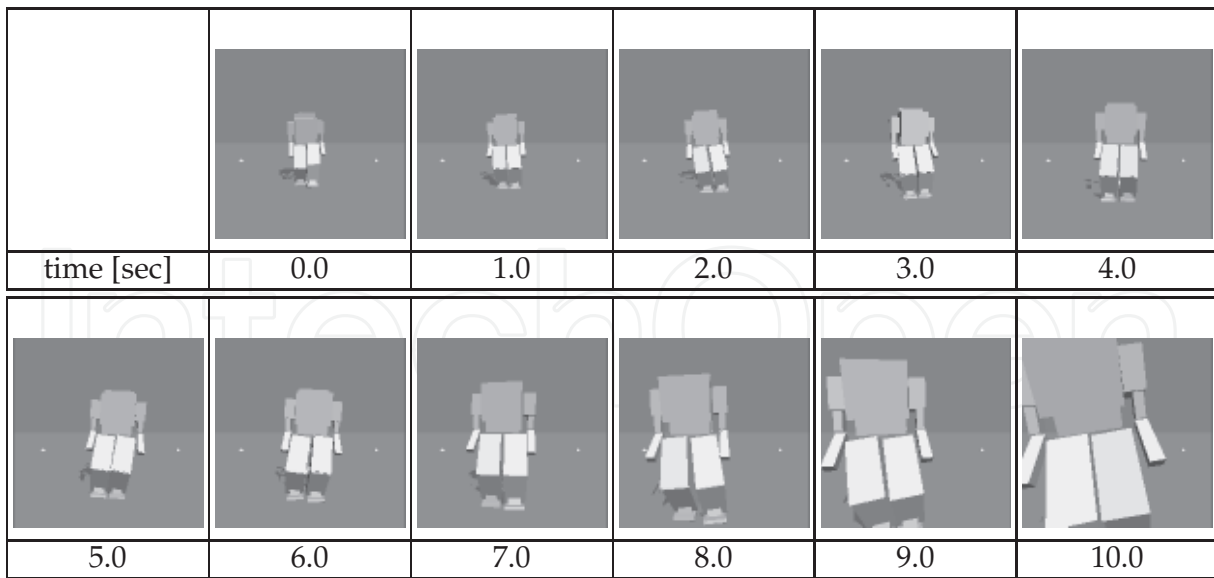
We determined the effects of the dynamic passivization of the joint control. In this experiment, we used a level ground.

Figure 16 shows the gaits over 10 seconds on a level ground. In this figure, the snapshots of the gait were traced every 1.0 seconds. Table 4 shows the travel distances, the sum total of the input torques, the locomotion costs. Our system that has the mechanism of passivization of joint control generated walking that was longer than that of CPG. The sum total of the input torques of CPG's walking is less than that of Our system's walking. However, the travel distance increased more than the increment of the consumption torque, and our system reduced the locomotion cost. We confirmed that our system generated energy efficient walking.

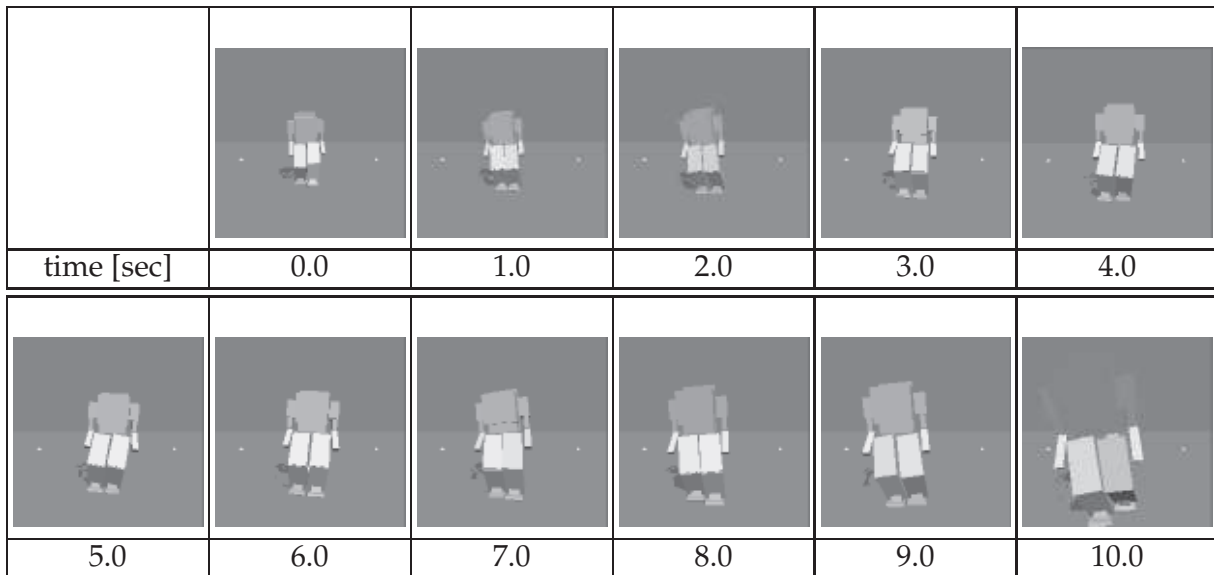
Figure 17 shows the trajectories of center of gravity of the robot (horizontal plane component) by the two methods. In this figure, the solid and broken lines show the trajectory of our system and CPG, respectively. The Stride of our system's gait is longer than that of CPG's gait, because our system appropriately nullifies the input torque in the swing leg. Therefore, our system generated walking that was longer than that of CPG.

5.2 Gait stability analysis

We determined the gait stability. We analyzed the gait stability using the lyapunov exponent (Alligood et al. (1996)). The lyapunov exponent is a method that measures a trajectory instability of reconstructed attractor. If a maximum lyapunov exponent λ_1 that was calculated by this analysis is positive and a smaller value, the result indicates that the system acquires a stable gait. In this section, the attractors were reconstructed with the longitudinal data of the body's center of gravity while walking. The time delays for attractor reconstruction were selected as the first zero of the autocorrelation function (Albano et al. (1988)). We set the embedding dimension $m = 3$ (Takens (1981)). Table 5 shows the maximum lyapunov exponent of the body's center of gravity. In this table, the maximum lyapunov exponents of our system's gait are smaller than those of CPG. The walking using our system is steadier than the CPG.



(a) Our system



(b) CPG

Fig. 16. Snapshots of 3D gaits

	Our system	CPG
λ_{1COG_y}	0.0027	0.0062
λ_{1COG_z}	0.0676	0.1085

Table 5. Maximum Lyapunov Exponent (3D walk)

6. Related work

In one of the mixture of active walking and PDW, there is walking that is called “ballistic walking”. Ballistic walking is supposed to be a human walking model suggested by Mochon & McMahon (1980). They got the idea from the observation of human walking data, in which the muscles of the swing leg are activated only at the beginning and the end of the swing phase. Ogino et al. (2003) proposed a motion control method for energy efficient walking with

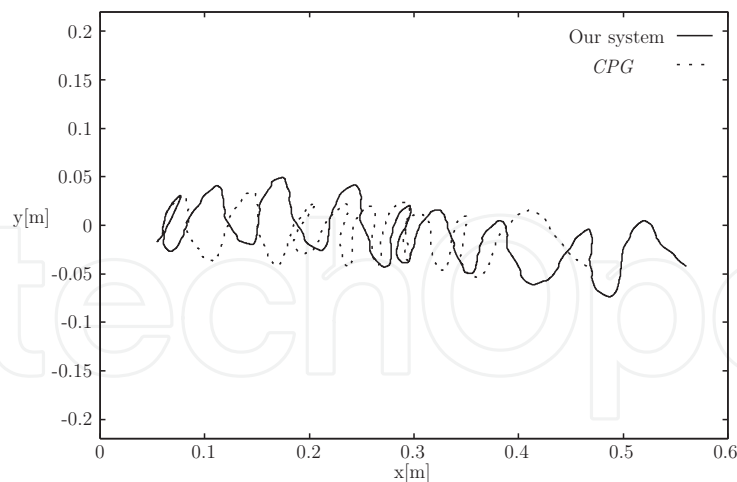


Fig. 17. Trajectories of center of gravity (horizontal plane)

ballistic walking. However, the method changes motion control statically. Even if the step time is changed, the passive phase period is always constant. Sugimoto & Osuka (2004) proposed a control method for quasi passive dynamic walking (Quasi-PDW). Quasi-PDW means that the robot usually does PDW without any input torque, and the actuators of the robot are used for ensuring walking stability only when the walking begins or when a disturbance occurs. Therefore, Quasi-PDW robots can generate energy efficient walking. However, Quasi-PDW is applicable to the robot whose dynamic characteristic suits to PDW. There are a lot of robots that can not satisfy a dynamic characteristic. Quasi-PDW robots have trouble to change the actions (e.g., changing of course, changing of speed, stop motion).

Our system dynamically changes joint control according to the pose information of robot and environment. Therefore, if the step time is changed, the robot can appropriately change joint control to passive. Our system need not to satisfy a dynamic characteristic to PDW, can easily change the actions.

7. Conclusions and future work

We described a motion control method for 2D and 3D biped robots based on a mixture of CPG and PDW, that is, dynamic passivization of joint control. We conducted walking control experiments to test the effectiveness of our method, and it demonstrated superior gaits. In gait stability analysis, we conducted that our system generated more stable gait than CPG's. We conducted walking control experiments on various downhill slopes, and our method was superior here as well. In experiments on uneven terrain, our method generated robust walking that was better than CPG's. We compared the robot and human gait, and our system had a trajectory that more closely modeled human walking than CPG.

In future work, we will create a motion control method that accounts for dynamic passivization of joint control other than in the swing leg. We will analyze the factor that the motion control using our system improved gait stability and robustness.

8. Acknowledgments

This work was supported in part by the Ministry of Education, Science, Sports and Culture, Grant-in-Aid for Scientific Research under grant #20700199.

9. References

- Albano, A. M., Muench, J., Schwarts, C., Mees, A. I. & Rapp, P. E. (1988). Singular-value decomposition and the grassberger-procaccia algorithm, *Physical Review A* **38**(6): 3017–3026.
- Alligood, K. T., Sauer, T. D. & Yorke, J. A. (1996). *Chaos: an introduction to dynamic systems*, Springer.
- Haruna, M., Ogino, M., Hosoda, K. & Asada, M. (2001). Yet another humanoid walking. -passive dynamic walking with torso under simple control-, *Proceedings of the 2001 IEEE/RSJ International Conference on Intelligent Robots and Systems (IROS-2001)*.
- Ishida, M., Kato, S., Kanoh, M. & Itoh, H. (2009a). Generating locomotion for biped robots based on the dynamic passivization of joint control, *Proceedings of the 2009 IEEE International Conference on Systems, Man, and Cybernetics (SMC 2009)*, pp. 3251–3256.
- Ishida, M., Kato, S., Kanoh, M. & Itoh, H. (2009b). Three dimensional bipedal walking locomotion using dynamic passivization of joint control, *Proceedings of the 2009 IEEE International Symposium on Micro-NanoMechatronics and Human Science (MHS 2009)*, pp. 580–585.
- Itoh, Y., Taki, K., Kato, S. & Itoh, H. (2004). A stochastic optimization method of cpg-based motion control for humanoid locomotion, *Proceedings of the IEEE Conference on Robotics, Automation and Mechatronics (RAM 2004)*, pp. 347–351.
- Kato, S. & Itoh, H. (2005). Soft computing approaches to motion control for humanoid robots, *International Symposium on Micro-Nano Mechatronics and Human Science*, pp. 47–52. (as an invited paper).
- Kotosaka, S. & Schaal, S. (2000). Synchronized robot drumming by neural oscillators, *Proceedings of the International Symposium on Adaptive Motion of Animals and Machines*.
- Matsuoka, K. (1985). Sustained oscillations generated by mutually inhibiting neurons with adaption, *Biological Cybernetics* **52**: 367–376.
- Matsuoka, K. (1987). Mechanisms of frequency and pattern control in the neural rhythm generators, *Biological Cybernetics* **56**: 345–353.
- McGeer, T. (1990). Passive dynamic walking, *The International Journal of Robotics Research* **9**(2): 62–81.
- Miki, M., Hiroyasu, T. & Ono, K. (2002). Simulated annealing with advanced adaptive neighborhood, *Proceedings of the 2nd International Workshop on Intelligent Systems Design and Applications (ISDA 2002)*, pp. 113–118.
- Miyakoshi, S., Taga, G., Kuniyoshi, Y. & Nagakubo, A. (1998). Three dimensional bipedal stepping motion using neural oscillators - towards humanoid motion in the real world -, *Proceedings of the 1998 IEEE/RSJ International Conference on Intelligent Robots and Systems (IROS'98)*, pp. 84–89.
- Mochon, S. & McMahon, T. A. (1980). Ballistic walking, *Journal of Biomechanics* **13**: 49–57.
- Murase, Y., Yasukawa, Y., Sakai, K. & et al. (2001). Design of a compact humanoid robot as a platform, *Proc. of the 19-th conf. of Robotics Society of Japan*, pp. 789–790. (in Japanese), <http://pr.fujitsu.com/en/news/2001/09/10.html>.
- Nakamura, T., Kato, S. & Itoh, H. (2005). A motion learning method consider joint stiffness for biped robots, *The 3rd International Conference on Computational Intelligence, Robotics and Autonomous Systems (CIRAS'2005)*, pp. CD-ROM (RH3–1).
- Ogino, M., Hosoda, K. & Asada, M. (2003). Learning energy efficient walking with ballistic walking, *Proceedings of the 2nd International Symposium on Adaptive Motion of Animal and Machines (AMAM'2003)*, pp. CD-ROM (ThP-I-5).

- Sugimoto, Y. & Osuka, K. (2004). Walking control of quasi passive dynamic walking robot "quartet iii" based on continuous delayed feedback control, *Proceedings of IEEE International Conference on Robotics and Biomimetics (Robio 2004)*.
- Taga, G. (1995a). A model of the neuro-musculo-skeletal system for human locomotion i. emergence of basic gait, *Biological Cybernetics* **73**: 97–111.
- Taga, G. (1995b). A model of the neuro-musculo-skeletal system for human locomotion ii. real-time adaptability under various constraints, *Biological Cybernetics* **73**: 113–121.
- Taga, G., Yamaguchi, Y. & Shimizu, H. (1991). Self-organized control of bipedal locomotion by neural oscillators in unpredictable environment, *Biological Cybernetics* **65**: 147–159.
- Takens, F. (1981). Detecting strange attractors in turbulence, *Lecture Notes in Mathematics* **898**: 366–381.
- Taki, K., Itoh, Y., Kato, S. & Itoh, H. (2004). Motion generation for bipedal robot using neuro-musculo-skeletal model and simulated annealing, *Proceedings of the IEEE Conference on Robotics, Automation and Mechatronics (RAM 2004)*, pp. 699–703.

IntechOpen



Biped Robots

Edited by Prof. Armando Carlos Pina Filho

ISBN 978-953-307-216-6

Hard cover, 322 pages

Publisher InTech

Published online 04, February, 2011

Published in print edition February, 2011

Biped robots represent a very interesting research subject, with several particularities and scope topics, such as: mechanical design, gait simulation, patterns generation, kinematics, dynamics, equilibrium, stability, kinds of control, adaptability, biomechanics, cybernetics, and rehabilitation technologies. We have diverse problems related to these topics, making the study of biped robots a very complex subject, and many times the results of researches are not totally satisfactory. However, with scientific and technological advances, based on theoretical and experimental works, many researchers have collaborated in the evolution of the biped robots design, looking for to develop autonomous systems, as well as to help in rehabilitation technologies of human beings. Thus, this book intends to present some works related to the study of biped robots, developed by researchers worldwide.

How to reference

In order to correctly reference this scholarly work, feel free to copy and paste the following:

Shohei Kato and Minoru Ishida (2011). Dynamic Joint Passivization for Bipedal Locomotion, Biped Robots, Prof. Armando Carlos Pina Filho (Ed.), ISBN: 978-953-307-216-6, InTech, Available from:
<http://www.intechopen.com/books/biped-robots/dynamic-joint-passivization-for-bipedal-locomotion>

INTECH
open science | open minds

InTech Europe

University Campus STeP Ri
Slavka Krautzeka 83/A
51000 Rijeka, Croatia
Phone: +385 (51) 770 447
Fax: +385 (51) 686 166
www.intechopen.com

InTech China

Unit 405, Office Block, Hotel Equatorial Shanghai
No.65, Yan An Road (West), Shanghai, 200040, China
中国上海市延安西路65号上海国际贵都大饭店办公楼405单元
Phone: +86-21-62489820
Fax: +86-21-62489821

© 2011 The Author(s). Licensee IntechOpen. This chapter is distributed under the terms of the [Creative Commons Attribution-NonCommercial-ShareAlike-3.0 License](#), which permits use, distribution and reproduction for non-commercial purposes, provided the original is properly cited and derivative works building on this content are distributed under the same license.

IntechOpen

IntechOpen